

Approach for Mechanical Isotropic Material Extrusion Printing

Authors Anna Verena Witt (M. Sc.)^a, Clemens Lieberwirth (M. Sc.)^b

^a NEW AIM3D GmbH Industriestraße 12, 18069 Rostock, Deutschland

^b NEW AIM3D GmbH Industriestraße 12, 18069 Rostock, Deutschland

https://doi.org/10.58134/fh-aachen-rte_2025_007

Zusammenfassung Diese Studie stellt einen neuen Ansatz zur Verringerung der anisotropen Materialeigenschaften bei Bauteilen aus dem Materialextrusionsverfahren (MEX) vor. Dabei wird die sogenannte Voxelfill-Methode genutzt, bei der statt der üblichen schichtweisen Ablage eine volumetrische Kammerfüllung erfolgt. Ziel ist es, isotrope Eigenschaften zu erreichen – auch bei faserverstärkten Kunststoffen. Untersucht wurden die mechanischen Eigenschaften von PETG-Proben mit 30 % Glasfaseranteil. Im Vergleich zum herkömmlichen Verfahren konnte die Anisotropie deutlich von 56,71 % auf 13,47 % reduziert werden.

Abstract This paper presents a novel approach to mitigate anisotropic material behavior in material extrusion (MEX) components, using fused granulate modeling (FGM) as fabrication technique and standard injection molding feedstock as material. This method, further named as Voxelfill disrupts the conventional layer-by-layer deposition by introducing a volumetric chamber filling technique and therefore aims to achieve isotropic properties in additive manufacturing (AM). This applies for both unfilled and fiber-reinforced thermoplastic polymers. The initial section of the paper articulates the motivation behind this study, providing an overview of the challenges posed by anisotropy in MEX processes. Following this, the Voxelfill process is briefly analyzed, with insights on its integration into slicing software and the hardware modifications necessary for implementation. The core focus of this study is to assess the mechanical performance of 30 % glass fiber-reinforced PETG parts by fabricating tensile test samples using the Voxelfill process and comparing them with specimens produced through conventional layer-by-layer printing. Results demonstrate that the Voxelfill process reduces anisotropy from 56.71 % to 13.47 %. These findings underscore the potential of the Voxelfill process to substantially mitigate anisotropic behavior in MEX components. The paper concludes with a discussion on future directions to further optimize and validate the benefits of the Voxelfill process, paving the way for enhanced reproducibility and performance in additive manufacturing applications.

1. Introduction and motivation

Material extrusion (MEX) is a prominent technique in additive manufacturing (AM) that builds objects layer-by-layer by extruding material, typically a thermoplastic filament or granulate, through a heated nozzle. The object is built on a platform as the extrusion nozzle moves horizontally and vertically, following a pre-determined path generated by a slicing software. By vertically moving the build platform the desired height a new layer is fused on top of the existing one, realizing the fabrication of complex parts layer-by-layer. A number of implementations of this process prove the versatility and accessibility, making it a fabrication technique that enables the creation of complex geometries with high material efficiency and therefore often finds application in rapid prototyping. [B1]

In 1989 Scott Crump patented a first apparatus for extrusion printing with thermoplastic polymers [P1] and material selection has expanded significantly over the last years. While multiple studies focus on printing polylactic acid (PLA) [J1], acrylonitrile butadiene styrene (ABS) [J2] and polyethylene terephthalate glycol (PETG) [J3], materials now include a range of high-strength composites, sinterable metallic or ceramic feedstock [J4] and biomaterial. In 2021 Rodzeń et al. included hydroxyapatite from bone to print with polyetheretherketone (PEEK) [J5]. More advanced materials like carbon- or glass fiber-reinforced polymers are enabling applications where higher strength and durability are required. In their study Wang, Peng et al. (2023) compared printability of PEEK reinforced with glass fiber and carbon fiber [J6] Vakharia et al. (2023) researched the printing of high temperature polyetherimide (PEI) for aerospace applications [J7].

However, the layer-by-layer deposition inherent to MEX also introduces certain limitations, such as anisotropic material properties [B2]. This anisotropy arises because the bonds between layers are weaker than the bonds within each layer, leading to directional weaknesses in mechanical strength [B2] As a result, MEX-produced parts can exhibit reduced performance under stress along the vertical built axis (mostly the z-axis) compared to the horizontal (x and y-axes). This effect was already proven 2002 by Ahn et al. when printing with ABS [J8] and further addressed by Zohdi, Nima and Young (2021) for a broader material selection [J9]. Guessasma et al. (2016) scrutinized the damage on printed parts due to anisotropic behavior [J10] Addressing anisotropy is crucial for applications requiring consistent mechanical strength and reliability across all directions. Challenging developers to overcome anisotropy has the potential to widen the application of MEX-parts from functional prototyping to tooling and end-user parts. Duty, Failla et al. (2019) introduced the idea of z-pinning to the conventional printing process while printing PLA and carbon reinforced PLA [J11]. They managed to show that the filling of channels spreading over multiple layers could enhance the mechanical strength by factor 3.5 [J11]. Nasirov et al. (2023) confirmed this theory by modelling the interfacial failure of z-pinned composites [J12]. A year earlier Bales and Walker et al. (2022) adapted to the challenge of z-pinning by making hardware adaptation to the printing nozzle [J13]. The potential for combining new materials and technologies is likely to further expand MEX's role across diverse industries, paving the way for highly customized, durable, and economically viable solutions in additive manufacturing. With this as motivation in mind the following sections of the paper closely introduce an approach to combining the existing MEX technologies with a method to reduce the anisotropy of printed parts.

2. Definitions

Fused granulate modelling (FGM) and fused filament fabrication (FFF) represent further subgroups of the MEX technology. While FGM uses granulates or pellets, which are commonly conveyed and melted by a screw extrusion unit, FFF uses filament within a gear extruder. In this research an FGM approach is chosen and will be compared with literature using FFF processes. FGM technology enables a greater variety of materials and larger component sizes while reducing material costs [J14]. At the same time, it is important to mention that the technological effort and machine costs are typically significantly higher than with the filament process. Despite this FGM also offers advantages in terms of production speed and the ability to use recycled materials [J15]. Due to these properties, FGM is increasingly favored in industrial applications, especially where large and robust components are required [J14]. A central area of research in the field of MEX is the investigation of the anisotropy of the mechanical properties, particularly the z-strength. MEX components exhibit a pronounced anisotropy due to their layered structure, with the strength in the z-direction (perpendicular to the layer plane) typically lower than in the x and y-directions. This anisotropy is caused by the weaker adhesion between the layers, which leads to reduced z-strength [B3]. Studies have shown that the optimization of printing parameters, such as printing temperature and layer height, as well as the use of post-processing techniques such as thermal post-treatment, can significantly improve the z-strength [B3]. While earlier approaches to the idea of filling volume chambers with thermoplastic material were limited to creating structures with holes [J11, J12, J13] that are causing a punctual connection of layers another process is introduced in the following. The Voxelfill process is described by generating a room-filling uniform structure of equally shaped volume elements, that a) have walls, forming the volume elements, that are printed layer-by-layer b) shifted in z-direction to each other c) are offset from their adjacent neighbors by half a height and d) are filled with thermoplastic material during the printing process every certain time, when the volume elements are reaching their top bordering surface. [P2]

To achieve these properties a variety of shapes is possible for the volume elements like cubic, hexagonal, rhombic dodecahedron or truncated octahedron. The shape of a truncated octahedron allows room filling arrangement without gaps, has a z-offset of half the height of the volume element and is close to a spherical shape, what is expected to be an optimal shape to fill with a fluid material. It is therefore chosen for further investigations as displayed in figure 1.

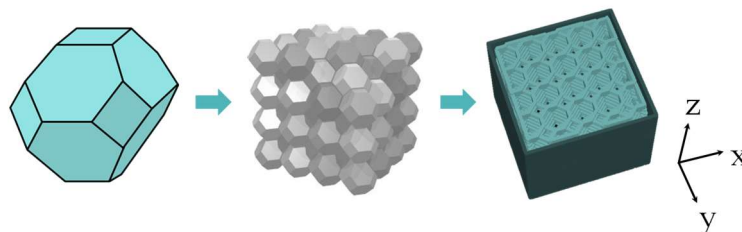


figure 1: Geometry of a truncated octahedron, the room filling arrangement of it and realization in slicer

Using the room filling arrangement of truncated octahedrons every volume element (here called voxel) is naturally offset to its adjacent neighbor by half a height of a voxel. This effect is used for the filling process. The printing of a Voxelfill part is achieved by repeating the following two steps:

- a. Printing the base structure with the voxels as hollow chambers,
- b. Fill the voxels at a defined z-height when the voxel shape is closing.

Because of the offset in z by half a voxel height only half the voxels in the filling layer are closing and are therefore filled. This amounts to a printed part where the layer-by-layer approach is disrupted in all three dimensions and no layer is running continuously through the geometry, while still creating a densely filled part.

3. Methodology

3.1. Material

For this research 3D printing pellets from Polymakers Polycore line, which are specifically designed for AM solutions were used. In order to investigate the influence of fiber distribution a reinforced PETG with short glass fibers (PolyCore PETG1013, Polymaker b.V., Houten, Neatherlands) was chosen. The material was dried at 70 °C for 4-6 hours prior to usage. Selected material properties are taken from the material data sheet and shown in the

table 1 below.

table 1: Properties of PolyCore PETG-1000 pellets taken from the data sheet [D1]

Parameter	Testing method	Value
Density [g/cm ³ at 21.5 °C]	ASTM D792	1.39
Glass transition temperature [°C]	DSC, 10 ° C/min	81

3.2. Slicer and printer hardware

The printer used was the CEM-printer ExAM255 (NEW AIM3D GmbH, Rostock, Germany) with a built volume of 255 x 255 x 255 mm³, vacuum bed and an extruder with a screw driven extrusion process. The platform can be heated to 140 °C, nozzle temperature can reach

425 °C and passive chamber heating was used.

Hardware adaption included a custom prototype nozzle with an elongated tip (diameter = 0.5 mm, Gühring KG, Leverkusen, Germany, see figure 2) and a water chiller miko Miniature Recirculating Chiller (technotrans systems GmbH, Baden-Baden, Germany) with a cooling capacity up to 400 W was used for active temperature control in the feeding zone of the extruder. To implement the Voxelfill process into a slicing process a Slicer software

was used. SlicEx is the whitelabel version of REAL Vision Pro Slicer (Creat it Real A/S, Aalborg, Denmark) and was at that time in a closed beta-testing phase. Slicing and design of the Voxelfill routine was done with the latest development version of SlicEx at that time (V 0.6.0).



figure 2: Prototype of custom nozzle for Voxelfill process made out of hardened steel

3.3. Process parameters

Preliminary to printing samples for testing the process parameters for PETG1013 were identified. The temperature was set to 270 °C to ensure good thermal bonding between the base structure and the filled material within the voxel. After setting the temperature and deciding on a fixed printing speed of 80 mm/s and layer height of 0.1 mm the flow through the nozzle was adapted by printing rectangular cubes with 20 % grid infill and measuring the line width until it reached the desired value of 0.6 mm. The flow factors for the perimeters and the walls of the volume chambers were adjusted accordingly. For a detailed description of the extrusion process and parameter optimization using the ExAM255 printer refer to Riaz, A. et al. (2022) who performed printing tests with a MIM feedstock [J4]. A list of the parameters used for printing are shown in table 2.

table 2: List of used process parameters for printing tensile test samples and density cubes

Parameter	Value	Unit
Bed temperature	70	°C
Feed zone temperature	45	°C
Nozzle temperature	270	°C
Nozzle diameter	0.5	mm
Layer height	0.1	mm
Line width	0.6	mm
Printing speed	80	mm/s
Extrusion flow factor perimeter	98	%
Extrusion flow factor ± 45°	98	%
Extrusion flow factor Voxelfill	120	%
Retraction	3	mm
Retraction speed	25	mm/s

3.4. Voxelfill method

As described in the definitions, the voxels are generated as a truncated octahedron. This is realized when printing 3D honeycomb infill type which creates a room filling bridged base of truncated octahedrons whose size depends on the infill percentage. The denser the infill is, the smaller the voxels get and vice versa. In this study the infill percentage is chosen as 26 % which leads to a voxel height of 3.7 mm and an idealistic volume of $V_{ideal} = 20.9 \text{ mm}^3$. Taking the line width of the printing into account, which reduces the ideal volume a realistic approximation of the volume is $V_{real} \approx 14.6 \text{ mm}^3$. In figure 3 a schematic overview of a filling routine is given. To fill a voxel, the nozzle of the extruder is placed at the coordinates of the center point of the smallest opening (figure 3-1) and is subsequently lowered into the voxel. In the lowered position material is extruded (figure 3-2) and after a short break the nozzles return to the starting position while extruding material into the top half of the voxel (figure 3-3). This is repeated for every closing voxel in the corresponding layer (figure 3-4). Since the voxels are offset in z for half a voxel height the filling is repeated every 1.85 mm. The amount of material as well as speed and waiting times were optimized in a trial-and-error approach prior to printing.

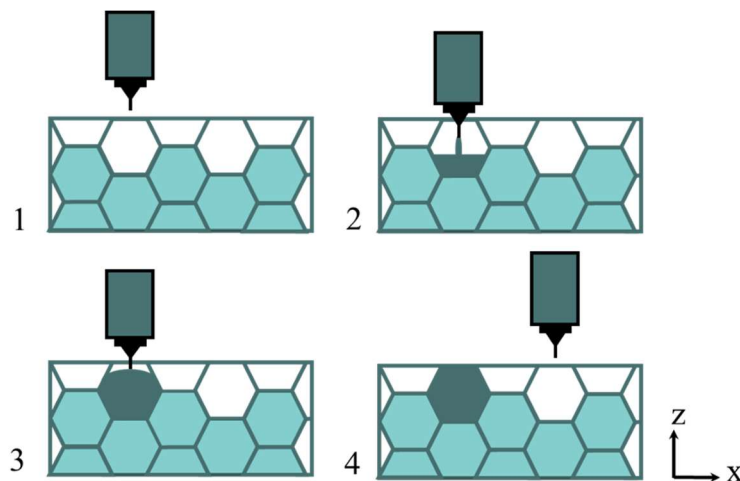


figure 3: Schematic visualization for the filling of a voxel.

3.5. Sample preparation

Printing

After the study to identify functional process parameters was finished, the samples were printed and prepared for tensile strength tests and density investigations. To obtain tensile samples cubes ($85 \times 20 \times 40 \text{ mm}^3$) with printing direction of the longest dimension first in x-direction and secondly z-direction were printed with 100 % conventional infill ($\pm 45^\circ$) and 26 % Voxelfill infill (3D honeycomb). This led to a printing sample amount of $n_1 = 4$. In the following chapters the four groups will be named as follows: x-conventional, z-conventional, x-voxel, z-voxel (referring first to the plane of testing and secondly the method of printing). After printing was done the number of $n_2 = 5$ tensile dog bone geometries were milled out of each printed block, which amounts to $n_{tot} = n_1 \cdot n_2 = 20$

tensile test samples. An illustration of the geometries and milling direction are shown in figure 4. This was decided since the border areas (refer to figure 3) were at that time not able to be filled with the slicer settings. Densely filled samples were chosen to test for tensile strength in order to have a better prove of concept.

To obtain samples for measuring the density cubes ($22 \times 22 \times 22 \text{ mm}^3$) were printed first conventionally ($n_3 = 5$) and secondly with Voxelfill ($n_4 = 5$). The process parameters were the same as for printing the tensile samples and after printing cubes of $10 \times 10 \times 10 \times 10 \text{ mm}^3$ were milled out of the center of the printed cubes. This amounts to $n_d = n_3 * n_4 = 10$ samples.

Milling

Dog bone geometries and density cubes were milled after printing with the Haas VF3-YT/50 (Haas Automation Inc., Oxnard, California, USA). The tool used was an HSC end mill VHM+Dia.HC W10° L63x20 z6 D8 and rotational speed of $V_r = 8100 \text{ rpm}$, feed speed $V_f = 1000 \text{ mm/min}$ and infeed values of 0.2 mm in z-direction and 0.6 mm in x direction (contour) were set. All samples were milled dry without water cooling and the settings were kept the same throughout all milling steps.

Embedding and grinding

The samples for microscopy testing and analyzing the fibers were cut from the tensile sample geometries after testing. Embedding was done in a cylindrical form with QPrep Qpox 94 hardener and QPrep Qpox 94 resin (ATM Qness GmbH, Mammelzen, Germany) mixed in ratio 1:2. Bubbles were removed under vacuum and the samples put into a refrigerator to cool and harden for more than 24 h. Additional sanding steps were done after embedding to ensure a smooth surface for microscopy. The Saphier 520 grinding machine (ATM Qness GmbH, Mammelzen, Germany) was used with sandpaper varying grits from 320 to 4000 and the samples were sanded for two minutes on each sandpaper with contact pressure of 10 N and rotational speed of 300 rpm .

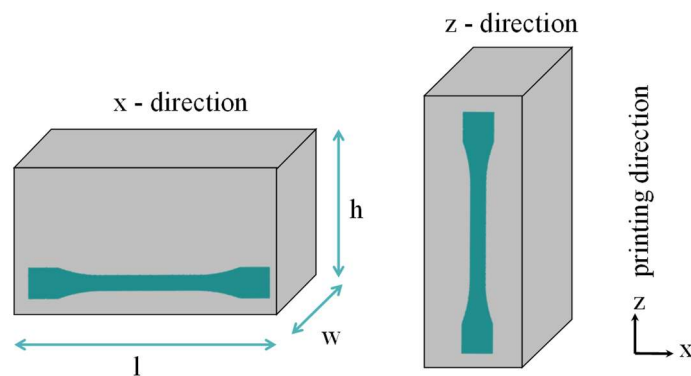


figure 4: Schematic illustration of printing direction of printing geometry for milling out tensile test dog bone samples.

3.6. Density measurements

Measurements for the density were performed with the Sartorius YDK01 density kit (*Sartorius AG, Göttingen, Germany*) at room temperature ($T_{\text{room}} = 20.7 \text{ }^{\circ}\text{C}$, $T_{\text{water}} = 21.2 \text{ }^{\circ}\text{C}$, $p_{\text{atm}} = 1032 \text{ hPa}$) using the Archimedes principle. Each of the five samples of the two groups (conventional, Voxelfill) were measured before testing.

3.7. Tensile testing

Each group (x-conventional, z-conventional, x-voxel, z-voxel) consists of five samples to guarantee statistical accuracy. The dog bone geometry was chosen to be type 1BA (ISO 527-2) to reduce printing and manufacturing time for sample preparation. The thickness of all samples was increased from $h \geq 2 \text{ mm}$ to $h = 4 \text{ mm}$ to have a more effective influence of the Voxelfill process by testing samples with a larger cross-sectional area. The geometric dimensions (in mm and naming according to norm ISO 527-2) are shown in table 3. [N1]

table 3: Geometric dimension of 1BA samples compared between ISO 527-2 and final dimensions in in research paper.

Parameter	Norm ISO 527-2	This research
l_3	≥ 75	78
l_1	30 ± 0.5	30
r	≥ 30	30
l_2	58 ± 2	58
b_2	10.0 ± 0.5	10
b_1	5.0 ± 0.5	5
h	≥ 2	4
L_0	25.0 ± 0.5	25
L	12	12

Tensile tests were performed with a velocity of 2 mm/min to achieve the same strain rate as in type 1A geometry with 5 mm/min. The universal testing machine inspekt duo (Hegewald und Peschke Meß-und Prüftechnik GmbH, Nossen, Germany) had a load frame up to 10 kN mounted. No extensometer was used to measure the Young's modulus, therefore this parameter will not be discussed within this publication. Before testing the thickness h and width b_1 of each sample were measured to ensure correct calculation of the cross section. All tests were performed at room temperature (20 °C).

3.8. Microscopy of fiber distribution

To obtain samples for analyzing the fiber distribution 10 mm long samples for the microscopy were cut out from the testing area of tensile samples after testing. Accordingly, the microscopy samples had a geometry of $4 \times 5 \times 10 \text{ mm}^3$ and images from microscopy can directly relate to mechanical values of the samples. Preparing the samples for microscopy included three steps 1) cutting out samples from the tensile bars, 2) embedding in resin and 3) sanding the embedded samples. Embedding and sanding was done

according to the description above. The samples were examined with the confocal microscope Olympus LEXT OLS4000 (Olympus K.K., Shinjuku, Japan) and photos were taken with the mounted CCD camera. The 5x and 10x objectives were used and the microscope images have a resolution of 1024 x 1024 pixels. Analysis of the image was done with the corresponding software package from Olympus.

4. Results

4.1. Difference in density measurements

Density measurements were performed for conventional and Voxelfill samples and compared. The results of the measurements are shown in table 4 below. The averaged value for the density of the conventionally printed samples was measured to be $\rho_c = 1.40 \text{ g/cm}^3$ with a percentage error of $e_c = 0.91\%$. In comparison to this, the average density of the Voxelfill samples reached $\rho_v = 1.30 \text{ g/cm}^3$ with a percentage error of $e_v = 6.25\%$. Standard deviation for measurements of five samples was $4.9\text{e-}9$ for conventional samples and 0.02 for Voxelfill samples.

table 4: Results for measuring the density of conventional and Voxelfill samples using the Archimedes principle

1	2	3	4	5	$\bar{\rho} \pm \sigma$
ρ in g/cm^3 for conventional samples					
1.40	1.41	1.40	1.40	1.40	$1.40 \pm 4.9\text{e-}9$
ρ in g/cm^3 for Voxelfill samples					
1.27	1.31	1.30	1.31	1.32	1.30 ± 0.02

4.2. Increase of tensile strength in z-direction

Tensile strength tests were carried out for the four groups of printing methods: x-conventional (x-c1 to x-c5), z-conventional (z-c1 to z-c5), x-voxel (x-v1 to x-v5) and z-voxel (z-v1 to z-v5). Results are shown in figure 5 to figure 7 and averaged values are given in

table 6. The conventionally printed samples reached an average tensile strength of 40.59 MPa and 10.44% of elongation in x-direction before failure. Meanwhile in z-direction the samples reached tensile strength of 17.67 MPa and strained to 1.55% , therefore showing an anisotropy of 56.71% in tensile strength and 85.15% in elongation at break. Samples that were printed with Voxelfill process reached a tensile strength of 35.78 MPa in x and 30.96 MPa in z-direction. This results in an anisotropy of 13.47% . Looking at the elongation at break, Voxelfill samples showed a percentual difference of only 4% between x and z-direction. Though the anisotropy dropped to 13.47% the absolute maximum of tensile strength decreased from 40.59 MPa by 4.81 MPa to a maximum of 35.78 MPa in x-direction which amounts to a 11.86% difference.

table 5: Averaged tensile strength, elongation at break, x-z anisotropy for conventional and Voxelfill samples.

Method	Rm [MPa]	σ [MPa]	Anisotropy [%]	ϵ [%]	deviation	Anisotropy [%]
x conventional	40.59	2.6	56.71	10.44	1.02	85.15
z conventional	17.67	2.54		1.55	0.19	
x - voxel	35.78	1.07	13.47	2.48	0.15	4.00
z - voxel	30.96	1.91		2.50	0.23	

table 6: Comparison of anisotropy values in different materials and strategies to reduce anisotropy.

Material	Anisotropy [%]	Strategy	Anisotropy after strategy [%]	Decrease in x [%]	ref
PLA	52.00	-	-	-	[32]
ABS	65.50	-	-	-	[33]
PLA	32.90	z-pinning	9.08	59.89	[8]
PLA-CF	32.72	z-pinning	29.32	65.18	[8]
PETG-GF	56.71	Voxelfill	13.47	11.86	

4.3. Fiber distribution

All twenty samples from tensile strength testing were analyzed with a confocal microscope, but only one image with 10-fold magnification for each of the groups was representatively selected to be discussed in this research paper. The results are shown in figure 8 and figure 9. For conventionally printed samples in x-direction fibers are distributed in a 45° angle and have an average length of 250 μm . The fibers in the conventionally printed Z-sample are seen as dots, meaning they have no orientation in Z-direction. Both conventionally printed images show pores ranging from 10-200 μm .

In figure 9 the fiber distribution in a voxel in the x-plane (left) and z-plane (right) is shown. Therefore, the angled fibers in figure 9 (left) are oriented in x. As demonstrated the border of the voxel (figure 9-A) is indicated by fibers $l_f > 150 \mu\text{m}$ that run parallel to each other. The figure 9 (right) visualizes the fiber distribution in a voxel in the z-plane, with the angled fibers in being inclined in z. In this orientation all angled fibers only exist within a voxel, while the border is being recognized by several dotted fibers, that are distributed in y-direction or horizontal fibers (0° angle to related to z) that are oriented in the x-plane. Pores (figure 9-B) with a length up to 400 μm can be seen in between voxel (figure 9-C) and border of the voxel (figure 9-A) in both images, indicating there are pores propagating along x and z-direction.

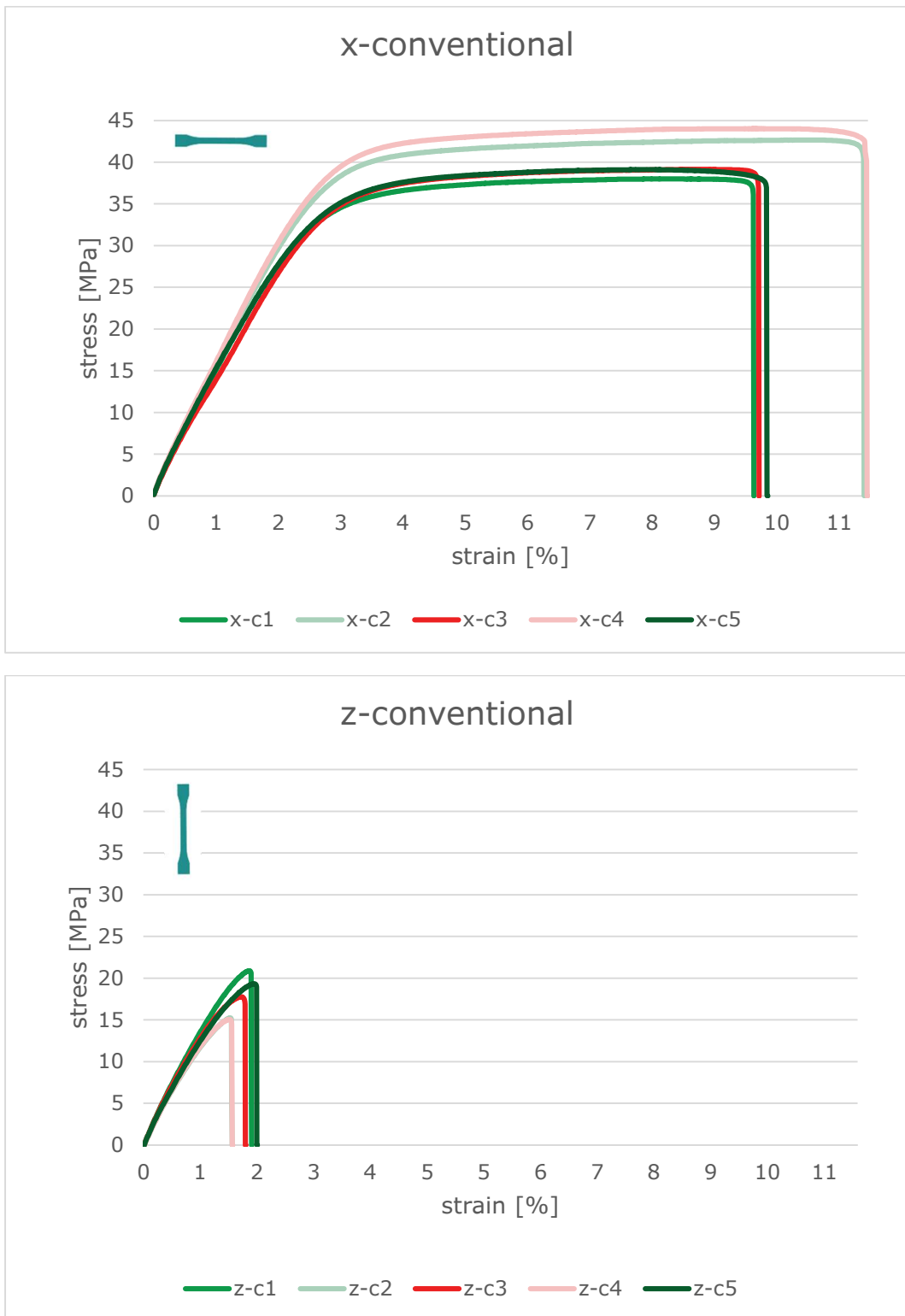


figure 5: Stress-strain curves of conventionally printed samples in x and z-direction with 100 % infill and angle of +45°

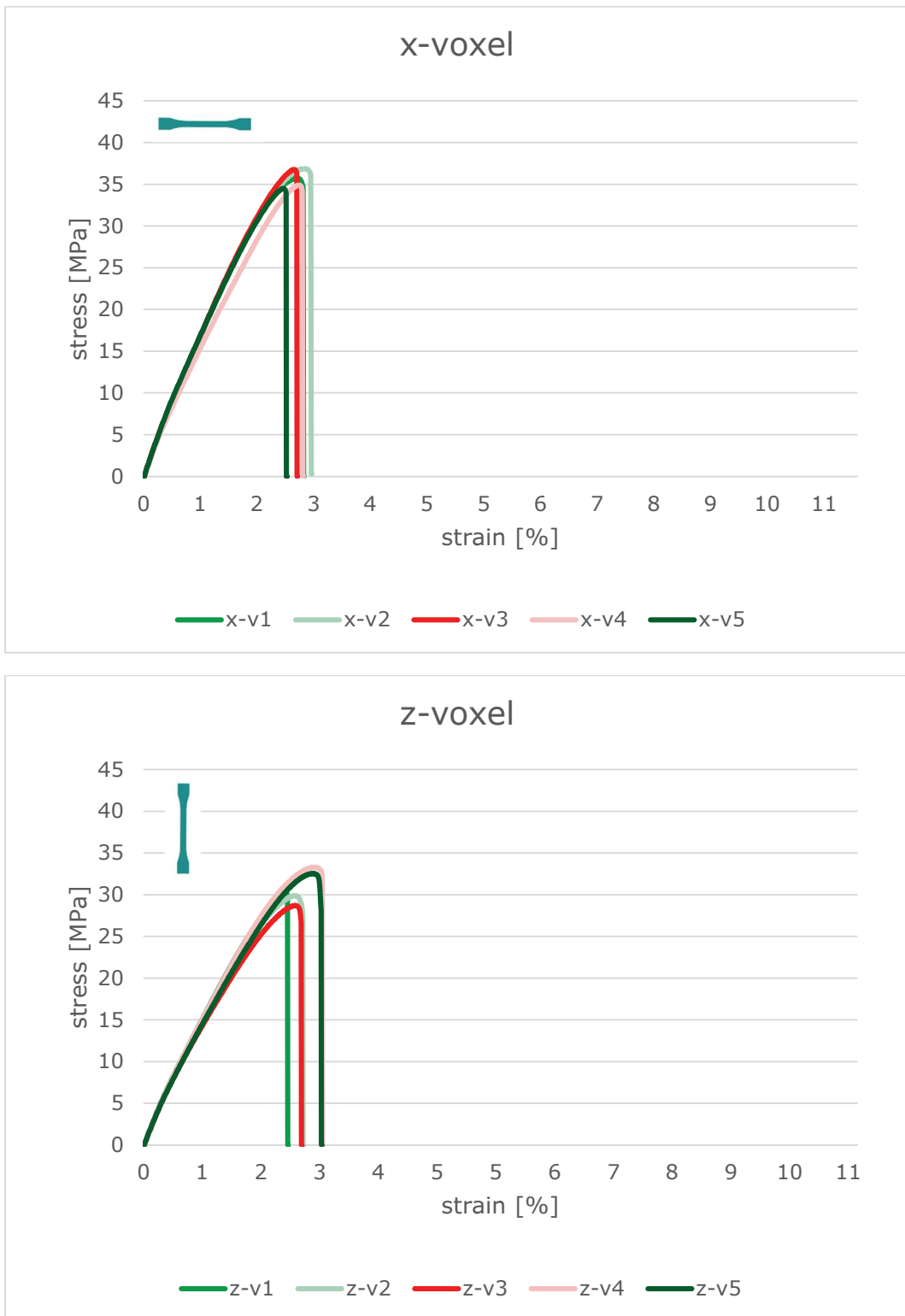


figure 6: Stress-strain curves of Voxelfill printed samples in x and z-direction with 26% infill

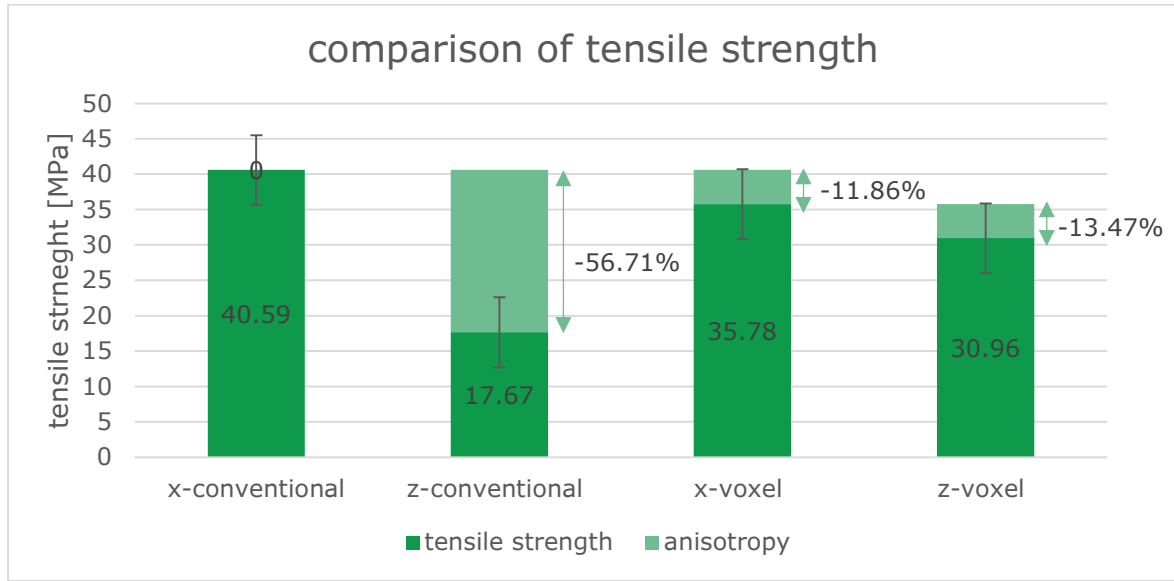


figure 7: Comparison of tensile strength and analysis of anisotropy between conventionally printed and Voxelfill samples in x and z-direction.

5. Discussion and error analysis

5.1. Density measurements

The averaged value for the density of the conventionally printed samples was measured to be $\rho_c = 1.40 \text{ g/cm}^3$, which is slightly higher than the value expected from the data sheet [D1] $\rho_d = 1.39 \text{ g/cm}^3$. By milling out the samples from the core of a bigger cube it was possible to eliminate typical pore gaps in between the perimeter and infill of the printed sample [J16, J17]. The slight overestimation of the density could be explained by air bubbles disrupting the fine measurement values taken in water and the percentage error of $e_c = 0.91 \%$ is negligible. In comparison to this, the average density of the Voxelfill samples reached $\rho_v = 1.30 \text{ g/cm}^3$ with a percentage error of $e_v = 6.30 \%$. The Voxelfill samples therefore reached 93.70 % of the expected density from the data sheet. Since Voxelfill samples showed a decreased density, it is to be assumed that pores and defects are enclosed within the structure.

5.2. Anisotropy in tensile strength

The results show a much lower anisotropy of 13.47 % in tensile strength for Voxelfill samples compared to conventionally printed samples with $\pm 45^\circ$ grid infill. The standard deviation for the groups x-voxel and z-voxel was also lower when measuring the tensile strength than it was for the groups x-conventional and z-conventional. A comparison of researched anisotropy is given in

table 6. Zohdi et al. (2024) investigated anisotropy of 65.50 % for layer height of 0.15 mm in ABS [J18]. When FFF printing PLA samples, Zhao et al. (2019) proved a 26.00 MPa decline in strength and calculated anisotropy of 52.00 % for a layer height of 0.1 mm [J19]. The z-pinning approach of Duty, Failla et al. (2019) [J11] showed promising results of reducing the anisotropy in FFF-printed PLA and PLA-CF samples. While anisotropy for

conventionally printed parts was 33 % it dropped to 9.08 % (PLA) and 29.32 % (PLA-CF) with z-pinning.

While Voxelfill samples gained in isotropic behavior they showed a 11.86 % drop in maximum tensile strength in x-direction compared to conventionally printed samples. A possible explanation are the identified voids in Voxelfill samples. Microscopy images specifically showed large pores in the boundary area (figure 9-B) between the printed 3D honeycomb infill and the filling in the voxel. Density measurements further proved it. Under tension less bonding between the layers leads to samples failing earlier compared to samples with less pores and higher density. It is to be said, that fibers increase the number of pores because they act as foreign body in the polymer matrix, suggesting that for homogeneous PETG material the decrease in strength would be less prominent [J6, J20]. A decrease in strength could also be identified using the z-pinning approach. The maximum tensile strength in x-direction decreased 65.18 % for 120 % z-pinned PLA-CF samples, showing a more distinctive reduction than for Voxelfill [J11].

As often explained in research the existence of pores and printing defects are defining factors why MEX printed parts show a decrease in strength and toughness. [J20, J21] Reducing the amount in both conventionally and Voxelfill samples would possibly further increase their mechanical performance. Additionally, the maximum x-strength is also affected by fiber distribution. For x-conventional samples most fibers are aligned in a 45° angle to the plane of load (see figure 8)

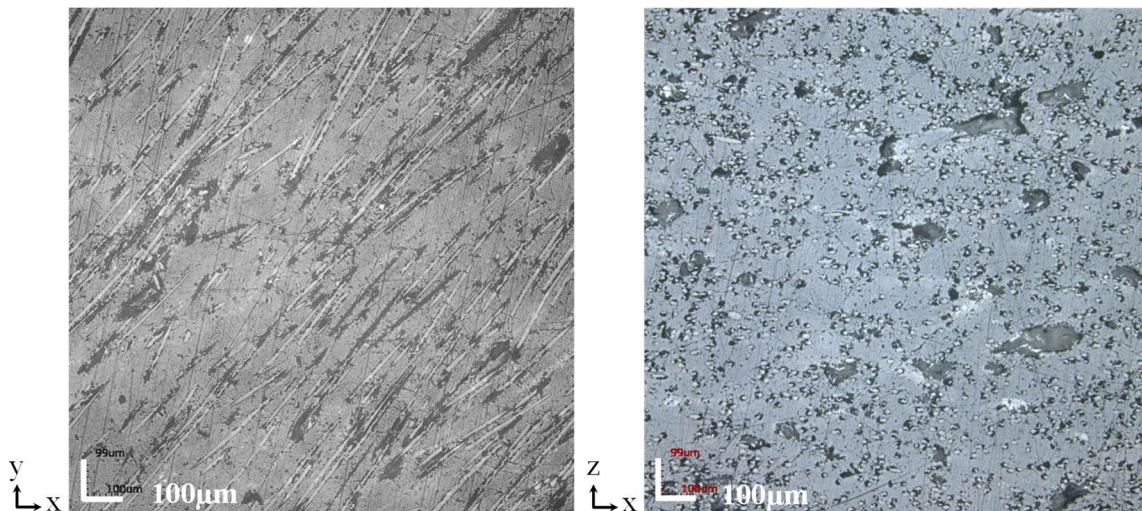


figure 8: Microscopy images (10 told magnification) of fiber distribution and pores in conventionally printed samples in x-direction (left) and z-direction (right).

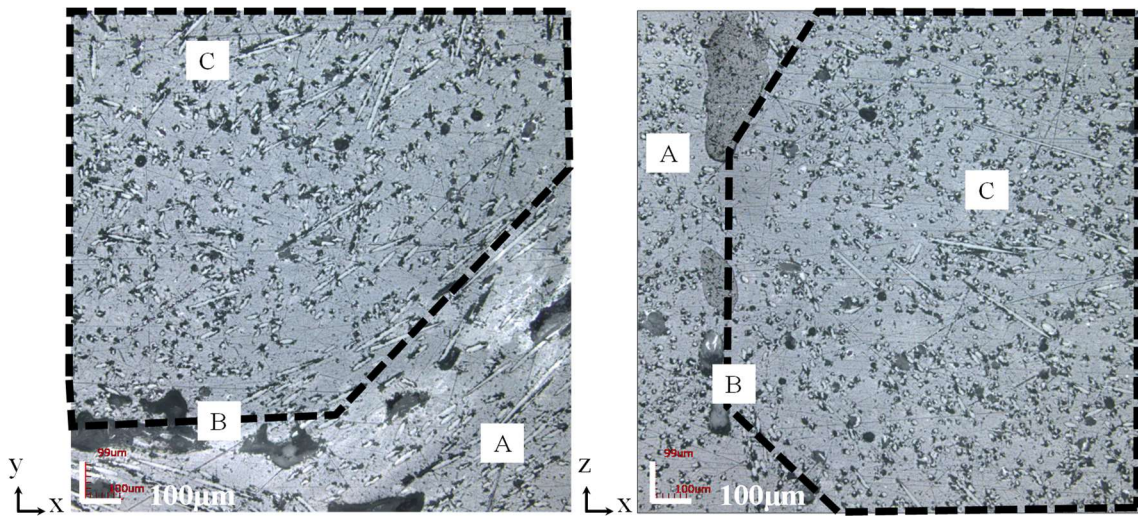


figure 9: Microscopy images (10 fold magnification) of fiber distribution and pores in Voxelfill printed samples in x-direction (left) and z-direction (right). Voxelarea is represented by the dotted line with A - voxel boundary area, B - voids in between voxel and boundary area and C - voxel area.

Ning, Cong et al. (2017) tested the influence of different infill angles on carbon fiber reinforced polymers mechanical performance [J22]. When more fibers were aligned in the direction of load (e.g. $90^{\circ}/0^{\circ}$ orientation) the strength increased while printing with an $\pm 45^{\circ}$ orientation the ductility increased. An unexpected increase in ductility could also be observed for x-conventional samples, while ductility for the other groups was much lower. From qualitatively comparing the microscopy images (figure 8-9), it can be concluded, that the amount of fibers being aligned to the axes of loading was higher in conventional samples than Voxelfill samples. Additionally, research with pure ABS showed that an infill angle of $\pm 45^{\circ}$ lead to a higher number of pores than $90^{\circ}/0^{\circ}$ samples [J18]. These points further explain the decrease in maximum tensile strength for Voxelfill samples. Since no information was given in the data sheet to the fabrication and testing of the tensile strength in injection molded samples no comparison can be made.

5.3. Pore and fiber distribution in microscopy images

Microscopy images of the conventionally printed samples show fiber orientation as would be expected from cutting the samples in xy and zx-printing plane. Refer to [J23] for a detailed analysis of 3-dimensional fiber orientation based on 2-dimensional REM images. As seen in figure 8 (left), the fibers are oriented in a 45° angle which agrees well with the infill pattern of $\pm 45^{\circ}$ grid infill, meanwhile in the zx-plane they can only be seen as dots. More pores can be found in the zx plane compared to the xy-plane. The image in x-direction shows one layer, while the image in z-direction spans over several printing layers with a height of $100 \mu\text{m}$ and therefore visualizes typical MEX printing inter-layer voids [J20]. Voids that are larger than half a layer height might be due to a temporary under extrusion or clogging of the nozzle.

What seems contradictory to the number of pores shown on the microscopic scale are the density measurements. The density calculations indicated that conventionally printed parts should reach up to 100 % density. The extrusion output with a screw-driven extruder is not linear to velocity and smaller geometries have travel moves with a shorter interval between acceleration and deceleration. In this dynamic printing behavior, a screw-driven extruder tends to extrude too much material and too little for larger geometries like the tensile blocks.

In figure 9 the xy-plane and zx-plane view of a voxel can be seen. Both voxel areas exhibit angled fibers that are distributed in either x or z. Even though the fibers were not counted it can be optically concluded that there are more and longer fibers distributed in x-direction rather than z-direction. This is also an explanation for the higher tensile strength in x compared to z, as identified in the tensile strength tests. In both xy and zx-plane large voids ($> 25000 \mu\text{m}^2$) are found between the voxel and the adjacent walls. A possible conclusion is that the amount of material filled into the voxel was not sufficient to fill the entire voxel. Additionally, the shrinkage of the material during cooling might separate contact areas with insufficient thermal bonding. The density measurements, which identified a lower density for Voxelfill samples than given in the data sheet, agree with the fact that larger pores can be found in Voxelfill samples compared to conventionally printed samples. It is to be highlighted that even though samples printed with the Voxelfill strategy had a lower density and larger number of voids, they performed more isotropic under tension. The decrease of 11.86 % in maximum tensile strength in x-direction is to be explained by the bigger voids.

5.4. Error in microscopy images

Because microscopy samples had to be cut into pieces all microscopy images were taken after performing tensile strength tests. This decision substantiated in the aim to get images directly related to strength values. This might have increased the size or modified the form of voids that have been identified in this paper. Since this procedure has been performed the same on all samples a qualitative comparison is still given. Future research should additionally focus on performing microscopy on non-tested samples to deeper analyze pore morphology.

6. Conclusion and outlook

This study successfully demonstrated the feasibility of the Voxelfill process. Samples were fabricated and systematically analyzed in terms of density, tensile strength, and fiber orientation. The introduction of voxels, subsequently filled with thermoplastic material during the printing process, resulted in a significant increase in tensile strength from 17.67 MPa to 30.96 MPa in the z-direction. Consequently, the anisotropy was reduced to 13.47 %. Notably, this improvement was achieved despite the lower density and the presence of larger and more numerous voids in Voxelfill samples compared to conventionally printed samples. Fiber analysis revealed that within the voxels, fibers were distributed across both the xy and zx-planes. Still a decrease of 11.85 % in maximum tensile strength in the x-direction due to voids could be identified.

Future investigations using PETG GF30 should prioritize a design of experiments (DOE) approach for optimizing process parameters and conducting a quantitative analysis of fiber content and orientation. Additional mechanical tests, such as compression and bending, are recommended to further evaluate and understand the anisotropic mechanical properties. Furthermore, the methodology should be expanded to incorporate a broader range of materials and hybrid material combinations.

The Voxelfill process demonstrates significant potential to advance MEX technology toward the production of near-isotropic components. This innovation could enable applications in markets previously constrained by anisotropic part performance. Moreover, the elimination of part orientation constraints during printing offers opportunities for enhanced surface quality and a reduction in the need for support structures, further improving the versatility and efficiency of the process.

7. Acknowledgement

This work was funded by the Ministry of Economics, Infrastructure, Tourism and Labour Mecklenburg Western Pomerania (funding code TBI-1-094-U-030). The authors express their sincere thanks to the Chair of Microfluidics of the University of Rostock, for technical support.

References

Books

- [B1] **Kumar, S.:** Additive Manufacturing Solutions (1st ed. 2022). *Imprint Springer. s.l. : Springer International Publishing, 2022.*
- [B2] **Srivastava, M., et al.:** Additive manufacturing. Fundamentals and advancements. Boca Boca Raton: London, New York: CRC Press, 2020.
- [B3] **Hirsch, A.; Paulus, M. S. ; Moritzer, E.:** Rissausbreitungsmechanismen in FDM-Verstärkungsstrukturen unter dynamischer Beanspruchung. Hans Albert Richard, Britta Schramm and Thomas Zipsner. *Additive Fertigung von Bauteilen und Strukturen: Neue Erkenntnisse und Praxisbeispiele.* Wiesbaden : Springer Fachmedien Wiesbaden, 2019, pp. 185–198.

Journals

- [J1] **Algarni, M.; Ghazali, S.:** Comparative Study of the Sensitivity of PLA, ABS, PEEK, and PETG's Mechanical Properties to FDM Printing Process Parameters. In: *Crystals. 2021, Vol. 11, 8.*
- [J2] **Portoaca, A., et al.:** Studies on the influence of FFF parameters on the tensile properties of samples made of ABS. In: *IOP Conference Series Materials Science and Engineering. 2022, Vol. 1, p. 1235.*
- [J3] **Erdaş, M. U., Yıldız, B. S. ;Yıldız, Ali R.:** Experimental analysis of the effects of different roduction directions on the mechanical characteristics

- of ABS, PLA, and PETG materials produced by FDM. In: *Materials Testing*. 2024, Vol. 66, 2, pp. 198–206.
- [J4] **Riaz, A., et al.:** Optimization of composite extrusion modeling process parameters for 3D printing of low-alloy steel AISI 8740 using metal injection moulding feedstock. In: *Materials & Design*. 2022, Vol. 219, p. 110814.
- [J5] **Rodzeń, K., et al.:** The Surface Characterisation of Fused Filament Fabricated (FFF) 3D Printed PEEK/Hydroxyapatite Composites. In: *Polymers*. 2021, Vol. 13, 18.
- [J6] **Wang, Peng, et al.:** Effects of FDM-3D printing parameters on mechanical properties and microstructure of CF/PEEK and GF/PEEK. In: *Chinese Journal of Aeronautics*. 2021, 34, pp. 236–246.
- [J7] **Vakharia, Ved S., et al.:** Multi-Material Additive Manufacturing of High Temperature Polyetherimide (PEI)-Based Polymer Systems for Lightweight Aerospace Applications. In: *Polymers*. 2023, Vol. 15, 3.
- [J8] **Ahn, SH., et al.:** Anisotropic material properties of fused deposition modeling ABS. In: *Rapid Prototyping Journal*. 2002, Vol. 8, 4, pp. 248–257.
- [J9] **Zohdi, N. ; Yang, R.C.:** Material Anisotropy in Additively Manufactured Polymers and Polymer Composites: A Review. In: *Polymers*. 2021, Vol. 13, 19.
- [J10] **Guessasma, S., et al.:** Anisotropic damage inferred to 3D printed polymers using fused deposition modelling and subject to severe compression. In: *European Polymer Journal*. 2016, Vol. 85, pp. 324–340.
- [J11] **Duty, C., et al.:** Z-Pinning approach for 3D printing mechanically isotropic materials. In: *Additive Manufacturing*. 2019, Vol. 27, pp. 175–184.
- [J12] **Nasirov, A., et al.:** Modeling the interfacial failure and resulting mechanical properties of z-pinned additively manufactured composites. In: *Materials Today Communications*. 2023, Vol. 35, p. 105735.
- [J13] **Bales, B., et al.:** Design and Use of a Penetrating Deposition Nozzle for Z-Pinning Additive Manufacturing. In: *International Solid Freeform Fabrication Symposium*. 2022, pp.1-10
- [J14] **Romani, A.; Levi, M.:** Large-Format Material Extrusion Additive Manufacturing for Circular Economy Practices: A Focus on Product Applications with Materials from Recycled Plastics and Biomass Waste. In: *Sustainability*. 2024, Vol. 16, 18.
- [J15] **Nguyen, P.Q.K., et al.:** Influences of printing parameters on mechanical properties of recycled PET and PETG using fused granular fabrication technique. In: *Polymer Testing*. 2024, Vol. 132, p. 108390.

- [J16] **Blok, L. G., et al.:** An investigation into 3D printing of fibre reinforced thermoplastic composites. In: *Additive Manufacturing*. 2018, Vol. 22, pp. 176–186.
- [J17] **Kechagias, J.; Zaoutsos, S.:** Effects of 3D-printing processing parameters on FFF parts' porosity: outlook and trends. In: *Materials and Manufacturing Processes*. 2024, Vol. 39, 6, pp. 804–814.
- [J18] **Zohdi, N.; Nguyen, P. Q. K. ; Yang, R.:** Evaluation on Material Anisotropy of Acrylonitrile Butadiene Styrene Printed via Fused Deposition Modelling. In: *Applied Sciences*. 2024, Vol. 14, 5, p. 1870.
- [J19] **Zhao, Y.; Chen, Y. ; Zhou, Y.:** Novel mechanical models of tensile strength and elastic property of FDM AM PLA materials: Experimental and theoretical analyses. In: *Materials & Design*. 2019, Vol. 181.
- [J20] **Ismail, K.I.; Yap, T. C.; Ahmed, R.:** 3D-Printed Fiber-Reinforced Polymer Composites by Fused Deposition Modelling (FDM): Fiber Length and Fiber Implementation Techniques. In: *Polymers*. 2022, Vol. 14, 21.
- [J21] **Wang, X., et al.:** Effect of Porosity on Mechanical Properties of 3D Printed Polymers: Experiments and Micromechanical Modeling Based on X-ray Computed Tomography Analysis. In: *Polymers*. 2019, Vol. 11, 7.
- [J22] **Ning, F., et al.:** Additive manufacturing of carbon fiber-reinforced plastic composites using fused deposition modeling: Effects of process parameters on tensile properties. In: *Journal of Composite Materials*. 2017, Vol. 51, 4, pp. 451–462.
- [J23] **Nargis, R. A. ; Jack, D. A.:** Fiber Orientation Quantification for Large Area Additively Manufactured Parts Using SEM Imaging. In: *Polymers*. 2023, Vol. 15, 13.

Norms

- [N1] **Standardisation, International Organisation for.** Plastics — Determination of tensile properties. *Part 2: Test conditions for moulding and extrusion plastics*. 2012. SO 527-2:2012.

Patents

- [P1] **Crump, S.S.:** *Apparatus and method for creating three-dimensional objects*. US5121329A US, 1989.
- [P2] **Lieberwirth, Clemens and Morrisin, Vincent.** *Method for the additive manufacturing of a component, using at least on volume chanber this is to be filled with a filler material*. EP4100235 (A1) EP, 2022.

Data Sheets

- [D1] **LLC, Polymaker.** *Polycore PETG-1013 Technical Data Sheet Ver 1.1*. 2021. <https://wiki.polymaker.com/polymaker-products/polycore-tm-pellets/products/polycore-tm-petg-1013>

Contact

Anna Verena Witt

Industriestraße 12

18069 Rostock

E-Mail: verena.witt@aim3d.de

WEB: www.aim3d.de

Clemens Lieberwirth

Industriestraße 12

18069 Rostock

E-Mail: clemens.lieberwirth@aim3d.de

WEB: www.aim3d.de